HHS Public Access

Author manuscript

Exp Mech. Author manuscript; available in PMC 2020 March 01.

Published in final edited form as:

Exp Mech. 2019 March ; 59(3): 327–336. doi:10.1007/s11340-018-00445-4.

Probing Endothelial Cell Mechanics Through Connexin 43 Disruption

M. M. Islam[1], **R. L. Steward Jr.**[1,2]

[1]Department of Mechanical and Aerospace Engineering

[2]Burnett School of Biomedical Sciences, College of Medicine, University of Central Florida, Orlando, FL

Abstract

The endothelium has been established to generate intercellular stresses and suggested to transmit these intercellular stresses through cell-cell junctions, such as VE-Cadherin and ZO-1, for example. Although the previously mentioned molecules reflect the appreciable contributions both adherens junctions and tight junctions are believed to have in endothelial cell intercellular stresses, in doing so they also reveal the obscure relationship that exists between gap junctions and intercellular stresses. Therefore, to bring clarity to this relationship we disrupted expression of the endothelial gap junction connexin 43 (Cx43) by exposing confluent human umbilical vein endothelial cells (HUVECs) to a low (0.2 μg/mL) and high (2 μg/mL) concentration of 2,5-dihydroxychalcone (chalcone), a known Cx43 inhibitor. To evaluate the impact Cx43 disruption had on endothelial cell mechanics we utilized traction force microscopy and monolayer stress microscopy to measure cell-substrate tractions and cell-cell intercellular stresses, respectively. HUVEC monolayers exposed to a low concentration of chalcone produced average normal intercellular stresses that were on average 17% higher relative to control, while exposure to a high concentration of chalcone yielded average normal intercellular stresses that were on average 55% lower when compared to control HUVEC monolayers. HUVEC maximum shear intercellular stresses were observed to decrease by 16% (low chalcone concentration) and 66% (high chalcone concentration), while tractions exhibited an almost 2-fold decrease under high chalcone concentration. In addition, monolayer cell velocities were observed to decrease by 19% and 35% at low chalcone and high chalcone concentrations, respectively. Strain energies were also observed to decrease by 32% and 85% at low and high concentration of chalcone treatment, respectively, when compared to control. The findings we present here reveal for the first time the contribution Cx43 has to endothelial biomechanics.

Keywords

Gap junctions; Connexin43; Intercellular stresses; Monolayer stress microscopy; traction force microscopy; endothelial cells; biomechanics

Corresponding Author: R. L. Steward Jr., Department of Mechanical and Aerospace Engineering College of Medicine, Burnett School of Biomedical Sciences University of Central Florida, Tel: 407-823-5608 Fax: 407-823-0208 rstewardjr@ucf.edu.

Introduction

Endothelial Cells (ECs) are critical for essentially every major vascular function within the body, which includes maintaining blood vessel integrity, supplying oxygen and nutrients to surrounding tissues, and regulating blood flow [1–4]. Proper functioning of the endothelium is crucial for vascular homeostasis and endothelial dysfunction can lead to life threatening conditions such as a stroke or heart attack [2,4,5]. As the innermost layer of the vasculature, the endothelium constantly experiences a plethora of biochemical and biomechanical stimulus [2,6–8]. For example, histamine and thrombin prompts, ECs to contract and increases endothelial permeability [13–15]. During angiogenesis, protease induced matrix degradation of existing micro-vessels results in generation of new capillary sprouts, enabling ECs to migrate into surrounding tissues and form new vessels [1,16]. Furthermore, several groups have showed that ECs can sense their extracellular matrix (ECM) stiffness and generate tractions accordingly [17–19]. In fact, in vitro experiments showed HUVEC contractions reduced in a floating collagen gel concentration of 3mg/mL but increased when collagen concentration decreased to 1.5 mg/mL [19].

The examples mentioned above highlight two biomechanical events that are essential to endothelial function, contraction and migration. In fact, both contraction and migration require the generation of tractions [20–22] and intercellular stresses [23–26]. We measured both intercellular stresses and tractions by utilizing monolayer stress microscopy [9,26–28] and traction force microscopy [22,29–31], respectively. While the cell-substrate traction stresses are mediated in part by focal adhesions(FAs) [10,32] and actomyosin contractility [11,12,33], intercellular stresses have been suggested to be transmitted through cell-cell junctions, specifically, adherens junctions (AJs) and tight junctions (TJs) [34,35]. Recent studies have suggested endothelial permeability to be linked to TJs [36] and AJs, which have in turn been suggested to function as mechanosensors capable of transmitting intercellular stresses [37]. Furthermore, endothelial intercellular stresses have been demonstrated to be responsive to endothelial barrier agonists such as thrombin and histamine and be cooperative over many cell distances [27]. These examples suggest endothelial cell intercellular stress transmission and generation to be influenced in part by cell-cell junctions, specifically TJs and AJs [38–40], but the role of gap junctions play in endothelial biomechanics is currently unknown.

Gap junctions are a unique family of cell-cell junction proteins that mechanically links adjacent cells and provides a physical pathway for electrical current and biomolecules to travel from cell to cell [41–43]. Endothelial cells primarily express the gap junctions Cx40, Cx37 and Cx43 [42–45] and deletion or mutation of these gap junctions has been demonstrated to have a range of vascular ramifications [41,44]. Such ramifications include increased risk of hypertension in mice as a result of Cx40 deletion [46] and structural abnormalities in the skin, testis, and intestine in mice [47] as a result of Cx40 and Cx37 genetic deletion. However, vascular complications yielded from Cx43 deletion are arguably the most severe since genetic deletion of Cx43 has been demonstrated to induce hypotension in mice [48] and subsequently influence multiple regulatory genes associated with vasculogenesis in mice [49]. In addition, Cx43 has been reported to be crucial for endothelial cell proliferation, migration [41,44,50] and monocyte-endothelial cell adhesion,

a crucial step in inflammation and the initiation and progression of atherosclerosis [42,45,51].

Although the above examples clearly suggest Cx43 to play a crucial role in vascular homeostasis, in doing so they also reveal the obscure relationship that exists between Cx43 and endothelial cell mechanics. Therefore, to bring clarity to the relationship between Cx43 and endothelial cell mechanics we investigated the role Cx43 plays in endothelial cell intercellular stress generation and traction generation by targeting Cx43. Endothelial cells were seeded as monolayers onto polyacrylamide gels and exposed to a low (0.2 μg/mL) and high (2 μg/mL) concentration of 2,5-dihydroxychalcone. 2,5-dihydroxychalcone has been documented to reduce only Cx43 expression in endothelial cells in a dose-dependent manner [52] and exhibit potent anti-inflammatory and anti-platelet effects [53,54] as well. Both tractions and intercellular stresses were calculated using traction force microscopy and monolayer stress microscopy and Cx43 inhibition at high concentration resulted in a significant decrease in average normal intercellular stresses, maximum shear intercellular stresses, and rms tractions.

Material and Methods

Cell culture

Human umbilical vein endothelial cells (HUVECs) were purchased commercially from ThermoFisher and cultured in medium 200 (ThermoFisher) supplemented with large vessel endothelial supplement (ThermoFisher) and 1% penicillin-streptomycin (Corning) on 0.1% gelatin (Sigma-Aldrich) coated flasks at 37°C and 5% CO_2. HUVECs were used at passages 8–9 for all experiments.

Polyacrylamide gel fabrication

Polyacrylamide (PA) gels were prepared as described previously [9]. Briefly, 35 mm petri dishes (Cellvis) were treated with a bind silane solution for 45 mins and then air-dried prior to gel polymerization. PA gel solution was prepared by mixing ultra-pure water, 40% acrylamide (Bio-Rad), 2% bis-acrylamide (Bio-Rad), and 0.5 μm diameter fluorescent, carboxylate-modified microspheres beads (Invitrogen). The gel solution was then de-gassed for 45 mins. Subsequently, ammonium persulfate and TEMED (N,N,N’,N’-tetramethylethane-1,2-diamine) was added to polymerize the gel on the treated petri dishes, yielding a gel height of ~100μm (supplementary figure 6) and stiffness of 1.2 kPa. A stiffness of 1.2 kPa was used as this stiffness closely mimics the stiffness of the healthy endothelium [55]).

Cellular micropattern preparation

Micropatterns were fabricated from thin polydimethylsiloxane (PDMS) sections as described previously [9,10]. Briefly, a thin layer of PDMS (Dow Corning) was first cured in a 100 mm petri dish by mixing silicon base with a curing agent (20:1) overnight at room temperature. After fabrication, a circular PDMS section (16mm diameter) was removed using a hole puncher and subsequently a 1.25 mm diameter biopsy punch (world precision instruments) was used to puncture holes. PDMS micropattern stamps were then placed on

top of PA gels and patterned gels were then treated with sulfosuccinimidyl-6-(4-azido-2-nitrophenylamino) hexanoate (Sulfo-SANPAH; Proteochem) dissolved in 0.1 M HEPES buffer solution (Fisher Scientific) and placed under a UV lamp for 8 mins. After SANPAH burning, patterned gels were treated with 0.1mg/ml of collagen I (Advanced Biomatrix) overnight at 4° C. The following day, excess collagen was removed and HUVECs were seeded at a concentration of ~50×10^4 cells/mL and were allowed to attach for an hour. After an hour, micropatterns were removed and HUVEC's were then allowed to form confluent monolayers for at least 36 hours prior to experimentation.

2,5 dihydroxychalcone treatment

2,5 dihydroxychalcone (chalcone) (Sigma-Aldrich) was dissolved in dimethylsulfoxide (DMSO), (Fisher Scientific) as a stock solution at a concentration of 187.5 μg/mL. For Cx43 disruption experiments the previously mentioned stock solution was further diluted in cell culture media to a final low concentration (0.2 μg/mL) and high concentration (2 μg/mL) of chalcone.

Time lapse microscopy

Phase contrast and fluorescent images were acquired every 5 minutes using a Zeiss inverted microscope with a 10X objective and Hamamatsu camera. Micropatterned HUVEC monolayers were initially imaged in chalcone-free medium for 1 hour. After this time chalcone-free media was replaced with cell culture medium supplemented with either a low or high chalcone concentration and HUVEC monolayers were subsequently imaged for an additional 5 hours. After this time, HUVEC monolayers were incubated with 10x trypsin for 10 minutes to remove cells from the gel surface. This allowed us to acquire a stress-free image of the gel top surface, which was used for traction calculations.

Immunohistochemistry

Micro-pattered, HUVEC monolayers were first fixed with 4% formaldehyde and incubated at 37°C for 15 mins, followed by permeabilization with 0.2% Triton-X 100 for 5 mins at 37°C. After permeabilization, HUVEC monolayers were incubated with a 2% BSA blocking solution at 37°C and subsequently incubated with the following primary antibodies; mouse monoclonal Cx43 antibody (CX-1B1, Thermo-fisher), mouse monoclonal Cx40 antibody (2F9A11, Thermo-fisher), rabbit polyclonal Cx37 antibody (42–4400, Thermo-fisher), mouse monoclonal ZO-1 antibody (ZO-1 1A12,Thermofisher), rabbit polyclonal VE-Cadherin antibody (PA5–19612, Thermo-fisher) overnight at 4°C. After this time, HUVEC monolayers were incubated with following secondary antibodies; Alexa Fluor 488 goat anti-mouse IgG (A-11001, Thermo-fisher) or Alexa Fluor 594 goat anti-rabbit IgG (A-110122, Thermo-fisher) for 2 hours. Alexa Fluor 594 phalloidin was used to stain for f-actin. Cells were mounted with fluoromount-G with DAPI, sealed under a coverslip, and imaged using a Zeiss Inverted microscope.

Traction force microscopy (TFM) and Monolayer stress microscopy (MSM)

Traction force microscopy and monolayer microscopy was used as described previously [9,22,26,29]. Briefly, substrate gel deformations produced by the cell was calculated using a

particle image velocimetry (PIV) routine [22] and cell-substrate forces were calculated using fourier transform traction force microscopy [22,29]. Intercellular stresses were calculated using monolayer stress microscopy as described previously [9,26]. In brief, monolayer stress microscopy applies a straightforward force balance required by Newton's law to give us the two-dimensional stress tensor within the entire cellular monolayer and by rotating the coordinate system we compute the maximum principal stresses (σ_{max}) and minimum principal stresses (σ_{min}) with their respective orientations. At each point of the monolayer we then computed average normal intercellular stress ($\sigma_{max} + \sigma_{min}$)/2 and maximum shear intercellular stress ($\sigma_{max} - \sigma_{min}$)/2.

Measurement of cell velocity

Cell velocity was measured from phase contrast images using a custom-written PIV routine in MATLAB (see supplementary figure 7). Briefly, our PIV routine was used to calculate window shifts between sequential images and then pixel shifts were converted into displacements by multiplying with the pixel to micron conversion factor. Displacements were then averaged for each time points and converted into velocity. Images were taken in a time interval of 5 mins for 6 hours.

Results

2,5 dihydroxychalcone reduces Cx43 expression

Before we investigated the influence Cx43 disruption via 2,5 dihydroxychalcone had on endothelial cell biomechanics we first wanted to investigate the influence 2,5 dihydroxychalcone had on Cx43 structure. Our results revealed fluorescent images of Cx43 structure under low chalcone concentration (figure 1d, e and f) to look almost structurally indistinguishable when compared to control groups (figure 1a, b and c). However, Cx43 structure under high chalcone concentration (figure 1g, h and i) was observed to decrease dramatically when compared to control conditions (figure 1), suggesting reduction of Cx43 expression by *2,5 dihydroxychalcone* to be concentration dependent. Our results agree with those reported previously by Lee et al. [52]. To confirm the specificity of the influence of chalcone on connexin 43 we performed additional experiments where endothelial monolayers were incubated with chalcone at the dosage observed to have maximal mechanical disruption (2 μg/mL). From these experiments we stained for ZO-1 (tight junction), VE-Cadherin (adherens junction), and the gap junctions Cx40 and Cx37. Fluorescent images of the previously mentioned junctional proteins of chalcone-treated monolayers were observed to be virtually indistinguishable, when compared to control monolayers (supplementary figure 3 & 4).

We also stained for F-actin to determine if Cx43 disruption influenced actin cytoskeletal structure and actin structure remained intact and similar for all chalcone treatment conditions (supplementary figure 5).

Cx43 disruption reduces intercellular stresses

Analysis of all results was performed over a cropped 500 μm x 500 μm section within the middle of the 1.25 mm micropatterned monolayer. We choose this cropping location as this

has been shown by us previously to eliminate any potential boundary effects induced by the micropattern [9]. Phase contrast images of control and chalcone treated conditions 30 minutes before chalcone treatment and after chalcone treatment (2 hours and 6 hours) are shown in figure 2. Thirty minutes prior to chalcone treatment, average normal intercellular stresses were largely tensile and fluctuated around 220 ± 66 Pa for control, low chalcone treated, and high chalcone treated HUVECs (figure 3a, d and g). Two hours after chalcone treatment average normal intercellular stresses were around 285 ± 75 Pa and 106 ± 4 Pa at low chalcone treatment (figure 3e) and high chalcone treatment (2 μg/mL) (figure 3h) conditions, while control monolayers were around 235 ± 18 Pa (figure 3b). After 6 hours, average normal intercellular stresses were observed to be around 266 ± 22 Pa, 149 ± 30 Pa, and 249 ± 29 Pa for 0.2 μg/mL chalcone treated monolayers (figure 3f), 2 μg/mL chalcone treated monolayers (figure 3i), and control monolayers (figure 3c), respectively. While the average normal intercellular stresses both increased and decreased under chalcone treatments, the maximum shear intercellular stresses decreased under both chalcone concentrations when compared to control conditions. Thirty minutes prior to chalcone treatment, maximum shear intercellular stresses were also tensile and fluctuated around 230 ± 60 Pa for control, low chalcone treated, and high chalcone treated HUVECs (figure 4a, d and g). After two hours, maximum shear intercellular stresses generated by endothelial cells exposed to a low dose chalcone and high dose chalcone treatment fluctuated around 227± 20 Pa (figure 4e) and 91 ± 6 Pa (figure 4h) relative to control conditions, which were around 270 ± 30 Pa (figure 4b), respectively. At 6 hours, maximum shear intercellular stresses generated by cells exposed to a low dose chalcone concentration were around 185 ± 10 Pa (figure 4f) and 156 ± 30 Pa for cells exposed to a high dose chalcone concentration (figure 4i). Maximum shear intercellular stresses generated by control monolayers fluctuated around 241 ± 30 Pa (figure 4c). On average, we observed a 17% and 6% increase in magnitude of average normal intercellular stresses with low chalcone treatment and a 55% & 40% decrease in magnitude of average normal intercellular stresses with high chalcone treatment when compared to control after 2 hours and 6 hours of experiment (figure 5a), respectively. At the same time, shear intercellular stresses decreased by 16% & 23% at low chalcone concentration and decreased by 66% & 35% at high chalcone concentration when compared to control after 2 hours and 6 hours of experiment (figure 5b), respectively. In addition, a rugged intercellular stress landscape was observed for both normal (supplementary figure 1) and shear (supplementary figure 2) intercellular stresses at before chalcone (supplementary figure 1&2a, d and g) and after 2 hours (supplementary figure 1&2b, e and h) and after 6 hours of experiment (supplementary figure 1&2c, f and i) and stresses also remained largely tensile in nature.

Cx43 disruption reduces rms tractions and strain energy

Prior to chalcone treatment (at 30 mins) root mean squared (rms) tractions for all chalcone treatment conditions fluctuated around 59 ± 11 Pa (figure 6a, d and g) and after 1 hour of chalcone treatment rms tractions fluctuated around 51 ± 8 Pa for low dose chalcone (figure 6e) and 18 ± 2 Pa for high dose chalcone (figure 6h) and 45 ± 9 Pa for control conditions (figure 6b). After 6 hours, rms tractions fluctuated around 50 ± 4 Pa for 0.2μg/mL chalcone treated (figure 6f), 20 ± 3 Pa for 2μg/mL chalcone treated (figure 6i) and 46 ± 5 Pa for control conditions (figure 6c), respectively. This revealed a slight increase of rms tractions at

low chalcone dose while high chalcone dose yielded an almost 2-fold decrease in rms tractions when compared to control conditions (figure 7a) after 6 hours of experiment.

In addition, Cx43 disruption decreased strain energy at both chalcone treatment concentrations. Strain energy magnitude was observed to be 28 ± 3 pJ (figure 7b) and cellular velocities were around 0.29 ± 0.004 μm/min (figure 8a, d and g) at about 30 mins of experiment onset. However, after 1 hour of chalcone treatment the strain energy decreased to 19 ± 2 pJ and 4 ± 1 pJ for low and high dose chalcone treatment, respectively. In addition, strain energy plateaued at 3 hours for the remaining period of the experiment (figure 7b).

Cx43 disruption reduces cell velocities

After an hour of chalcone treatment cell velocities were 0.25 ± 0.003 μm/min for 0.2μg/mL chalcone treatment (figure 8e), 0.20 ± 0.005 μm/min for 2μg/mL chalcone treatment (figure 8h) and 0.31 ± 0.002 μm/min under control conditions (figure 8b). After 6 hours, cell velocities fluctuated around 0.27 ± 0.001 μm/min for 0.2μg/mL chalcone treatment (figure 8f), 0.17 ± 0.002 μm/min for 2μg/mL chalcone treatment (figure 8i) and 0.21 ± 0.003 μm/min for control conditions (figure 8c), respectively. While we observed around a 19% and 35% decrease in cell velocities after an hour of treatment for low and high chalcone dose respectively, after 6 hours of experiment low dose treated monolayers exhibited 22% increase in cell velocities compared to control (figure 9).

Discussion

In this paper, we report here for the first time how endothelial mechanics are influenced by the gap junction Cx43. We believe these findings will have implications into many Cx43-related biomechanical cellular processes. For example, during in vitro cell migration Cx43 expression was found to increase and contribute to the movement of the endothelial sheet as a collective via increased cell-cell coupling [44,50,56]. In our experiments we observed that endothelial monolayers exposed to a high concentration of chalcone decreased cell velocities significantly. In addition, Cx43 has also been suggested to be essential to endothelial barrier function in addition to tight junctions and adherens junctions [35,57]. Here, we report a notable reduction in strain energy as well as a significant decrease in maximum shear intercellular stresses and average normal intercellular stresses generated by the endothelial monolayer in the presence of chalcone. Taken together, our results suggest to us that endothelial monolayer mechanical strength and/or endothelial barrier function could be potentially enhanced or diminished by targeting Cx43 communication and expression.

Our results also reveal a surprising increase in normal intercellular stresses and rms tractions compared to control conditions with a low dose of chalcone treatment. Both maximum (σ_{max}) and minimum principal stresses (σ_{min}) were found to be higher for low concentration chalcone treatment compared to control which in turn showed higher average normal intercellular stresses and lower maximum shear stresses at low chalcone treatment condition compared to control (see supplementary figure 8). While the exact reason for this increase is unknown, it is possible that this low dose of chalcone treatment had a brief transient effect on endothelial mechanics. In addition, previous reports have suggested Cx43 to work in concert [41,44] with other gap junctions (Cx40 or Cx37). Therefore, it is possible that

additional endothelial gap junctions may be compensating for the perturbed Cx43 expression and function we have observed in this study.

Conclusion

The importance of Cx43 in vasculature research is undeniable and has been a research interest for long time. There have been a host of recent reports showing direct effect of Cx43 on vascular physiology and pathology [41,42,44]. However, to our best knowledge, there have been no reports relating endothelial mechanics, specifically intercellular stresses with Cx43. As we probe this complex interplay between Cx43 and endothelial stress generation, we believe our results will provide insights into how Cx43 communication influences endothelial permeability, barrier strength as well as leading to a greater understanding of overall endothelial mechanics.

Supplementary Material

Refer to Web version on PubMed Central for supplementary material.

Acknowledgements

This work was supported by the University of Central Florida start-up funds and the National Heart, Lung, And Blood Institute of the National Institute of Health under award K25HL132098.

References

1. Al-Soudi A, Kaaij MH, Tas SW (2017) Endothelial cells: From innocent bystanders to active participants in immune responses. Autoimmun Rev 16 (9):951–962. doi:10.1016/j.autrev.2017.07.008 [PubMed: 28698091]
2. Rajendran P, Rengarajan T, Thangavel J, Nishigaki Y, Sakthisekaran D, Sethi G, Nishigaki I (2013) The vascular endothelium and human diseases. Int J Biol Sci 9 (10):1057–1069. doi:10.7150/ijbs.7502 [PubMed: 24250251]
3. Wallez Y, Huber P (2008) Endothelial adherens and tight junctions in vascular homeostasis, inflammation and angiogenesis. Biochim Biophys Acta 1778 (3):794–809. doi:10.1016/j.bbamem.2007.09.003 [PubMed: 17961505]
4. Widlansky ME, Gokce N, Keaney JF Jr., Vita JA (2003) The clinical implications of endothelial dysfunction. J Am Coll Cardiol 42 (7):1149–1160 [PubMed: 14522472]
5. Hadi HA, Carr CS, Al Suwaidi J (2005) Endothelial dysfunction: cardiovascular risk factors, therapy, and outcome. Vasc Health Risk Manag 1 (3):183–198 [PubMed: 17319104]
6. Islam MM, Beverung S, Steward R Jr (2017) Bio-Inspired Microdevices that Mimic the Human Vasculature. Micromachines 8 (10). doi:10.3390/mi8100299
7. Lu D, Kassab GS (2011) Role of shear stress and stretch in vascular mechanobiology. J R Soc Interface 8 (63):1379–1385. doi:10.1098/rsif.2011.0177 [PubMed: 21733876]
8. Warren KM, Islam MM, LeDuc PR, Steward R (2016) 2D and 3D Mechanobiology in Human and Nonhuman Systems. ACS Applied Materials & Interfaces 8 (34):21869–21882. doi:10.1021/acsami.5b12064 [PubMed: 27214883]
9. Steward R, Tambe D, Hardin CC, Krishnan R, Fredberg JJ (2015) Fluid shear, intercellular stress, and endothelial cell alignment. American Journal of Physiology - Cell Physiology 308 (8):C657–C664. doi:10.1152/ajpcell.00363.2014 [PubMed: 25652451]
10. Steward RL Jr., Cheng CM, Wang DL, LeDuc PR (2010) Probing cell structure responses through a shear and stretching mechanical stimulation technique. Cell Biochem Biophys 56 (2–3):115–124. doi:10.1007/s12013-009-9075-2 [PubMed: 20033625]

11. Steward RL Jr., Cheng CM, Ye JD, Bellin RM, LeDuc PR (2011) Mechanical stretch and shear flow induced reorganization and recruitment of fibronectin in fibroblasts. Sci Rep 1:147. doi: 10.1038/srep00147 [PubMed: 22355663]
12. Steward RL Jr., Tan C, Cheng CM, LeDuc PR (2015) Cellular force signal integration through vector logic gates. J Biomech 48 (4):613–620. doi:10.1016/j.jbiomech.2014.12.047 [PubMed: 25614090]
13. Ashina K, Tsubosaka Y, Nakamura T, Omori K, Kobayashi K, Hori M, Ozaki H, Murata T (2015) Histamine Induces Vascular Hyperpermeability by Increasing Blood Flow and Endothelial Barrier Disruption In Vivo. PLoS One 10 (7):e0132367. doi:10.1371/journal.pone.0132367 [PubMed: 26158531]
14. Lum H, Malik AB (1996) Mechanisms of increased endothelial permeability. Can J Physiol Pharmacol 74 (7):787–800
15. Rabiet MJ, Plantier JL, Rival Y, Genoux Y, Lampugnani MG, Dejana E (1996) Thrombin-induced increase in endothelial permeability is associated with changes in cell-to-cell junction organization. Arterioscler Thromb Vasc Biol 16 (3):488–496 [PubMed: 8630677]
16. van Hinsbergh VW, Koolwijk P (2008) Endothelial sprouting and angiogenesis: matrix metalloproteinases in the lead. Cardiovasc Res 78 (2):203–212. doi:10.1093/cvr/cvm102 [PubMed: 18079100]
17. Chiquet M (1999) Regulation of extracellular matrix gene expression by mechanical stress. Matrix Biol 18 (5):417–426 [PubMed: 10601729]
18. Hosseini Y, Agah M, Verbridge SS (2015) Endothelial cell sensing, restructuring, and invasion in collagen hydrogel structures. Integr Biol (Camb) 7 (11):1432–1441. doi:10.1039/c5ib00207a [PubMed: 26379187]
19. Sieminski AL, Hebbel RP, Gooch KJ (2004) The relative magnitudes of endothelial force generation and matrix stiffness modulate capillary morphogenesis in vitro. Exp Cell Res 297 (2): 574–584. doi:10.1016/j.yexcr.2004.03.035 [PubMed: 15212957]
20. Fournier MF, Sauser R, Ambrosi D, Meister JJ, Verkhovsky AB (2010) Force transmission in migrating cells. J Cell Biol 188 (2):287–297. doi:10.1083/jcb.200906139 [PubMed: 20100912]
21. Lange JR, Fabry B (2013) Cell and tissue mechanics in cell migration. Exp Cell Res 319 (16): 2418–2423. doi:10.1016/j.yexcr.2013.04.023 [PubMed: 23664834]
22. Trepat X, Wasserman MR, Angelini TE, Millet E, Weitz DA, Butler JP, Fredberg JJ (2009) Physical forces during collective cell migration. Nature Physics 5:426. doi:10.1038/ nphys126910.1038/nphys1269https://www.nature.com/articles/nphys1269#supplementary-informationhttps://www.nature.com/articles/nphys1269#supplementary-information
23. De Pascalis C, Etienne-Manneville S (2017) Single and collective cell migration: the mechanics of adhesions. Mol Biol Cell 28 (14):1833–1846. doi:10.1091/mbc.E17-03-0134 [PubMed: 28684609]
24. Gov N (2011) Cell mechanics: moving under peer pressure. Nat Mater 10 (6):412–414. doi: 10.1038/nmat3036
25. Perrault CM, Brugues A, Bazellieres E, Ricco P, Lacroix D, Trepat X (2015) Traction Forces of Endothelial Cells under Slow Shear Flow. Biophys J 109 (8):1533–1536. doi:10.1016/j.bpj. 2015.08.036 [PubMed: 26488643]
26. Tambe DT, Hardin CC, Angelini TE, Rajendran K, Park CY, Serra-Picamal X, Zhou EH, Zaman MH, Butler JP, Weitz DA, Fredberg JJ, Trepat X (2011) Collective cell guidance by cooperative intercellular forces. Nat Mater 10 (6):469–475. doi:10.1038/nmat3025 [PubMed: 21602808]
27. Hardin C, Rajendran K, Manomohan G, Tambe DT, Butler JP, Fredberg JJ, Martinelli R, Carman CV, Krishnan R (2013) Glassy dynamics, cell mechanics, and endothelial permeability. J Phys Chem B 117 (42):12850–12856. doi:10.1021/jp4020965 [PubMed: 23638866]
28. Tambe DT, Croutelle U, Trepat X, Park CY, Kim JH, Millet E, Butler JP, Fredberg JJ (2013) Monolayer Stress Microscopy: Limitations, Artifacts, and Accuracy of Recovered Intercellular Stresses. PLOS ONE 8 (2):e55172. doi:10.1371/journal.pone.0055172 [PubMed: 23468843]
29. Butler JP, Tolić-Nørrelykke IM, Fabry B, Fredberg JJ (2002) Traction fields, moments, and strain energy that cells exert on their surroundings. American Journal of Physiology-Cell Physiology 282 (3):C595–C605. doi:10.1152/ajpcell.00270.2001 [PubMed: 11832345]

30. Cho Y, Young Park E, Ko E, Park J-S, Shin J (2016) Recent advances in biological uses of traction force microscopy, vol 17. doi:10.1007/s12541-016-0166-x

31. Hardin CC, Chattoraj J, Manomohan G, Colombo J, Nguyen T, Tambe D, Fredberg JJ, Birukov K, Butler JP, Del Gado E, Krishnan R (2018) Long-range stress transmission guides endothelial gap formation. Biochem Biophys Res Commun 495 (1):749–754. doi:10.1016/j.bbrc.2017.11.066 [PubMed: 29137986]

32. Elineni KK, Gallant ND (2011) Regulation of cell adhesion strength by peripheral focal adhesion distribution. Biophys J 101 (12):2903–2911. doi:10.1016/j.bpj.2011.11.013 [PubMed: 22208188]

33. Mierke CT, Fischer T, Puder S, Kunschmann T, Soetje B, Ziegler WH (2017) Focal adhesion kinase activity is required for actomyosin contractility-based invasion of cells into dense 3D matrices. Sci Rep 7:42780. doi:10.1038/srep42780 [PubMed: 28202937]

34. Bazzoni G, Dejana E (2004) Endothelial cell-to-cell junctions: molecular organization and role in vascular homeostasis. Physiol Rev 84 (3):869–901. doi:10.1152/physrev.00035.2003 [PubMed: 15269339]

35. Gulino-Debrac D (2013) Mechanotransduction at the basis of endothelial barrier function. Tissue Barriers 1 (2):e24180. doi:10.4161/tisb.24180 [PubMed: 24665386]

36. Tarbell JM (2010) Shear stress and the endothelial transport barrier. Cardiovasc Res 87 (2):320–330. doi:10.1093/cvr/cvq146 [PubMed: 20543206]

37. le Duc Q, Shi Q, Blonk I, Sonnenberg A, Wang N, Leckband D, de Rooij J (2010) Vinculin potentiates E-cadherin mechanosensing and is recruited to actin-anchored sites within adherens junctions in a myosin II–dependent manner. The Journal of Cell Biology 189 (7):1107 [PubMed: 20584916]

38. DeMaio L, Chang YS, Gardner TW, Tarbell JM, Antonetti DA (2001) Shear stress regulates occludin content and phosphorylation. Am J Physiol Heart Circ Physiol 281 (1):H105–113. doi:10.1152/ajpheart.2001.281.1.H105 [PubMed: 11406474]

39. Liu Z, Tan JL, Cohen DM, Yang MT, Sniadecki NJ, Ruiz SA, Nelson CM, Chen CS (2010) Mechanical tugging force regulates the size of cell-cell junctions. Proc Natl Acad Sci U S A 107 (22):9944–9949. doi:10.1073/pnas.0914547107 [PubMed: 20463286]

40. Ng MR, Besser A, Brugge JS, Danuser G (2014) Mapping the dynamics of force transduction at cell-cell junctions of epithelial clusters. Elife 3:e03282. doi:10.7554/eLife.03282 [PubMed: 25479385]

41. Figueroa XF, Duling BR (2009) Gap junctions in the control of vascular function. Antioxid Redox Signal 11 (2):251–266. doi:10.1089/ars.2008.2117 [PubMed: 18831678]

42. Nielsen MS, Axelsen LN, Sorgen PL, Verma V, Delmar M, Holstein-Rathlou NH (2012) Gap junctions. Compr Physiol 2 (3):1981–2035. doi:10.1002/cphy.c110051 [PubMed: 23723031]

43. Sohl G, Willecke K (2004) Gap junctions and the connexin protein family. Cardiovasc Res 62 (2):228–232. doi:10.1016/j.cardiores.2003.11.013 [PubMed: 15094343]

44. Haefliger JA, Nicod P, Meda P (2004) Contribution of connexins to the function of the vascular wall. Cardiovasc Res 62 (2):345–356. doi:10.1016/j.cardiores.2003.11.015 [PubMed: 15094354]

45. Marquez-Rosado L, Solan JL, Dunn CA, Norris RP, Lampe PD (2012) Connexin43 phosphorylation in brain, cardiac, endothelial and epithelial tissues. Biochim Biophys Acta 1818 (8):1985–1992. doi:10.1016/j.bbamem.2011.07.028 [PubMed: 21819962]

46. de Wit C, Roos F, Bolz SS, Pohl U (2003) Lack of vascular connexin 40 is associated with hypertension and irregular arteriolar vasomotion. Physiol Genomics 13 (2):169–177. doi:10.1152/physiolgenomics.00169.2002 [PubMed: 12700362]

47. Simon AM, McWhorter AR (2002) Vascular abnormalities in mice lacking the endothelial gap junction proteins connexin37 and connexin40. Dev Biol 251 (2):206–220 [PubMed: 12435353]

48. Liao Y, Day KH, Damon DN, Duling BR (2001) Endothelial cell-specific knockout of connexin 43 causes hypotension and bradycardia in mice. Proc Natl Acad Sci U S A 98 (17):9989–9994. doi:10.1073/pnas.171305298 [PubMed: 11481448]

49. Walker DL, Vacha SJ, Kirby ML, Lo CW (2005) Connexin43 deficiency causes dysregulation of coronary vasculogenesis. Dev Biol 284 (2):479–498. doi:10.1016/j.ydbio.2005.06.004 [PubMed: 16039638]

50. Kwak BR, Pepper MS, Gros DB, Meda P (2001) Inhibition of endothelial wound repair by dominant negative connexin inhibitors. Mol Biol Cell 12 (4):831–845 [PubMed: 11294890]

51. Yuan D, Sun G, Zhang R, Luo C, Ge M, Luo G, Hei Z (2015) Connexin 43 expressed in endothelial cells modulates monocyteendothelial adhesion by regulating cell adhesion proteins. Mol Med Rep 12 (5):7146–7152. doi:10.3892/mmr.2015.4273 [PubMed: 26324251]

52. Lee Y-N, Yeh H-I, Tian T-Y, Lu W-W, Ko Y-S, Tsai C-H (2002) 2′,5′-Dihydroxychalcone down-regulates endothelial connexin43 gap junctions and affects MAP kinase activation. Toxicology 179 (1):51–60. doi:10.1016/S0300-483X(02)00289-5 [PubMed: 12204542]

53. Hsieh HK, Lee TH, Wang JP, Wang JJ, Lin CN (1998) Synthesis and anti-inflammatory effect of chalcones and related compounds. Pharm Res 15 (1):39–46 [PubMed: 9487544]

54. Lin CN, Lee TH, Hsu MF, Wang JP, Ko FN, Teng CM (1997) 2',5'-Dihydroxychalcone as a potent chemical mediator and cyclooxygenase inhibitor. J Pharm Pharmacol 49 (5):530–536 [PubMed: 9178190]

55. Stroka KM, Aranda-Espinoza H (2011) Endothelial cell substrate stiffness influences neutrophil transmigration via myosin light chain kinase-dependent cell contraction. Blood 118 (6):1632–1640. doi:10.1182/blood-2010-11-321125 [PubMed: 21652678]

56. Pepper MS, Montesano R, el Aoumari A, Gros D, Orci L, Meda P (1992) Coupling and connexin 43 expression in microvascular and large vessel endothelial cells. American Journal of Physiology-Cell Physiology 262 (5):C1246–C1257. doi:10.1152/ajpcell.1992.262.5.C1246

57. Nagasawa K, Chiba H, Fujita H, Kojima T, Saito T, Endo T, Sawada N (2006) Possible involvement of gap junctions in the barrier function of tight junctions of brain and lung endothelial cells. J Cell Physiol 208 (1):123–132. doi:10.1002/jcp.20647 [PubMed: 16547974]

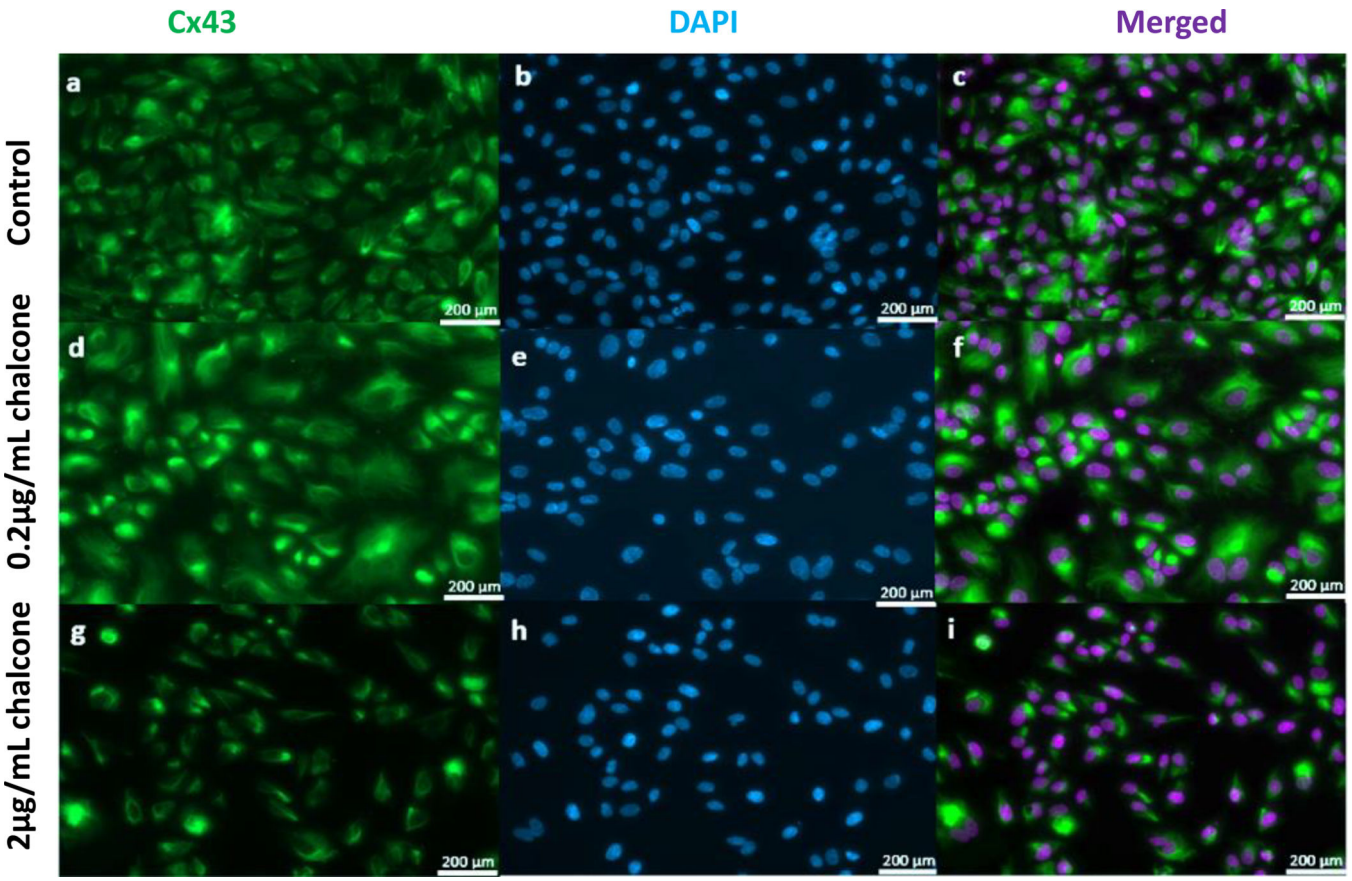

Figure 1:

Effect of chalcone treatment on Cx43 structure. Immunostaining was performed in HUVEC monolayers after 6 hours of chalcone treatment. Green color represents Cx43 and Blue represents DAPI. Figure labels are as follows- control (a, b, and c), 0.2 µg/mL chalcone treated cells (d, e, and f) and 2µg/mL chalcone treated cells (g, h, and i). (obj: 20x; scale bar = 200 µm).

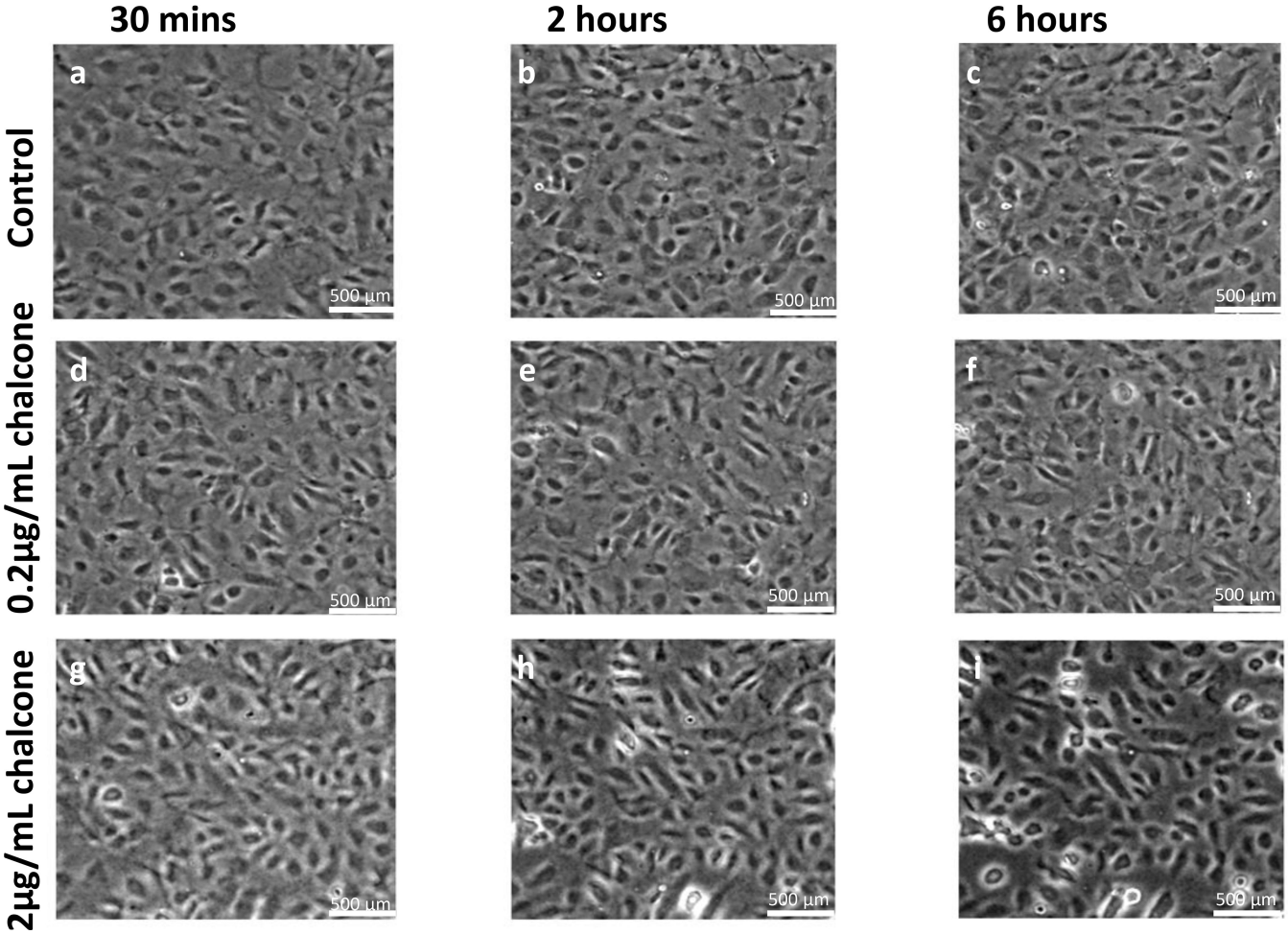

Figure 2:

Phase contrast images of HUVEC monolayers after Cx43 disruption. Control phase contrast images of HUVECs at 30 mins (a), 2 hours (b) and 6 hours (c). Phase contrast images of HUVECs treated with 0.2µg/mL chalcone at 30 mins (d), 2 hours (e) and 6 hours (f). Phase contrast images of HUVECs treated with 2µg/mL chalcone at 30 mins (g), 2 hours (h) and 6 hours (i). Scale bar 500 × 500 µm.

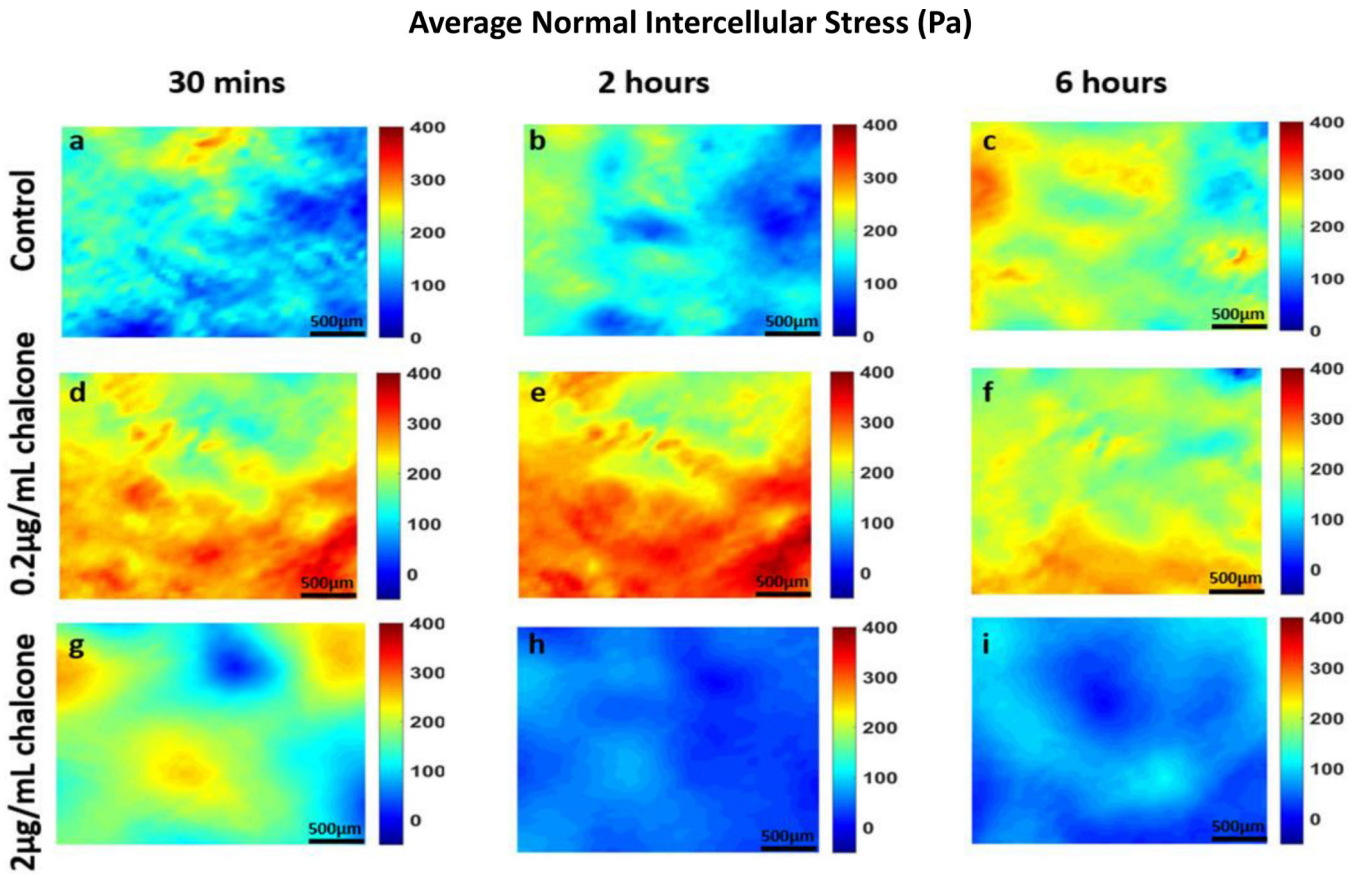

Figure 3:

Average normal intercellular stresses (Pa) of HUVEC monolayers during Cx43 inhibition. Figure labels show average normal intercellular stresses of HUVECs at 30 mins (a), 2 hours (b) and 6 hours (c) of control HUVECs and at 30 mins (d), 2 hours (e) and 6 hours (f) of HUVECs treated with 0.2µg/mL chalcone and at 30 mins (g), 2 hours (h) and 6 hours (i) of HUVECs treated with 2µg/mL chalcone. Scale bar 500 × 500 µm.

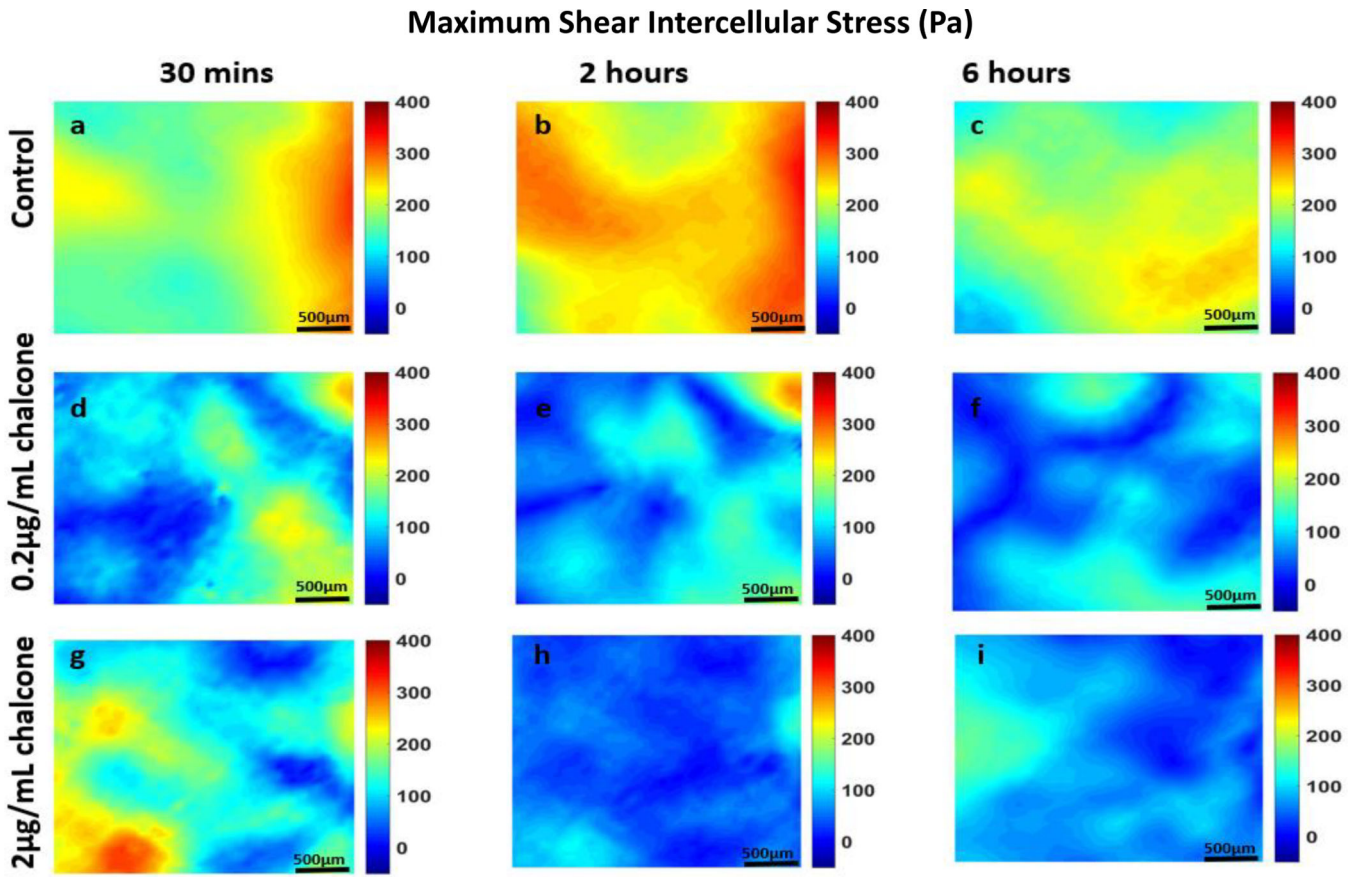

Figure 4:

Maximum shear intercellular stresses (Pa) of HUVEC monolayers during Cx43 inhibition. Figure labels show maximum shear intercellular stresses of HUVECs at 30 mins (a), 2 hours (b) and 6 hours (c) of control HUVECs and at 30 mins (d), 2 hours (e) and 6 hours (f) of HUVECs treated with 0.2µg/mL chalcone and at 30 mins (g), 2 hours (h) and 6 hours (i) of HUVECs treated with 2µg/mL chalcone. Scale bar 500 × 500 µm.

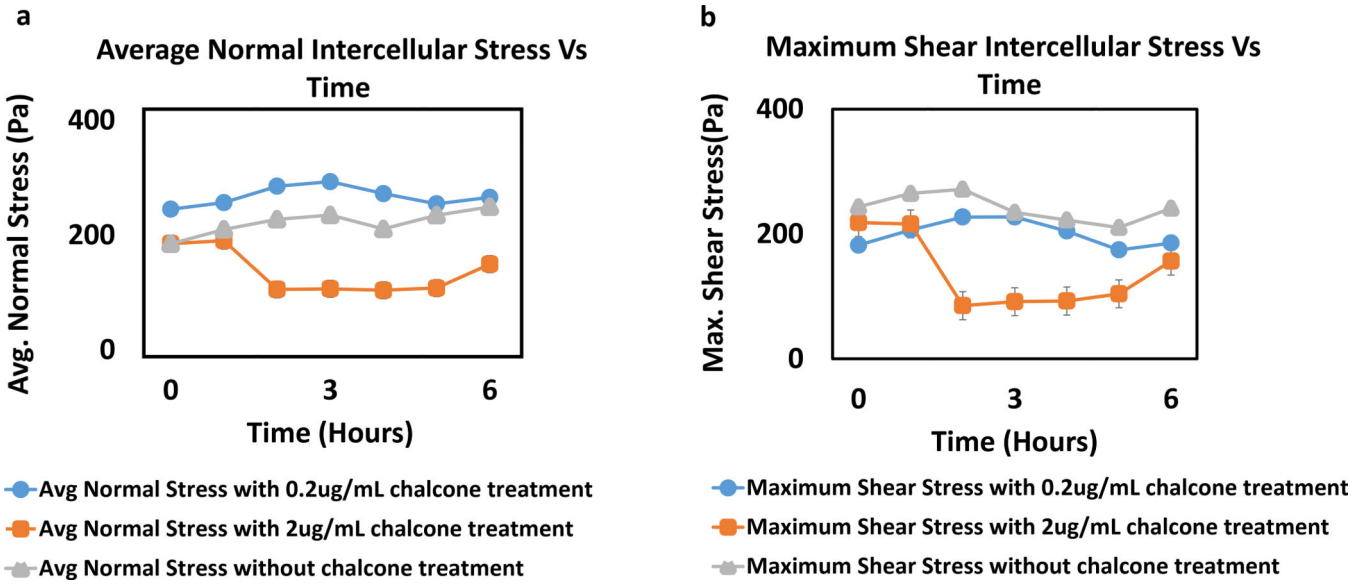

Figure 5:

Comparison of average normal intercellular stress(Pa) (a) and maximum shear intercellular stress(Pa) (b) of HUVEC monolayers in both chalcone treated (0.2 μg/mL and 2 μg/mL) and control conditions. Error bars show standard error.

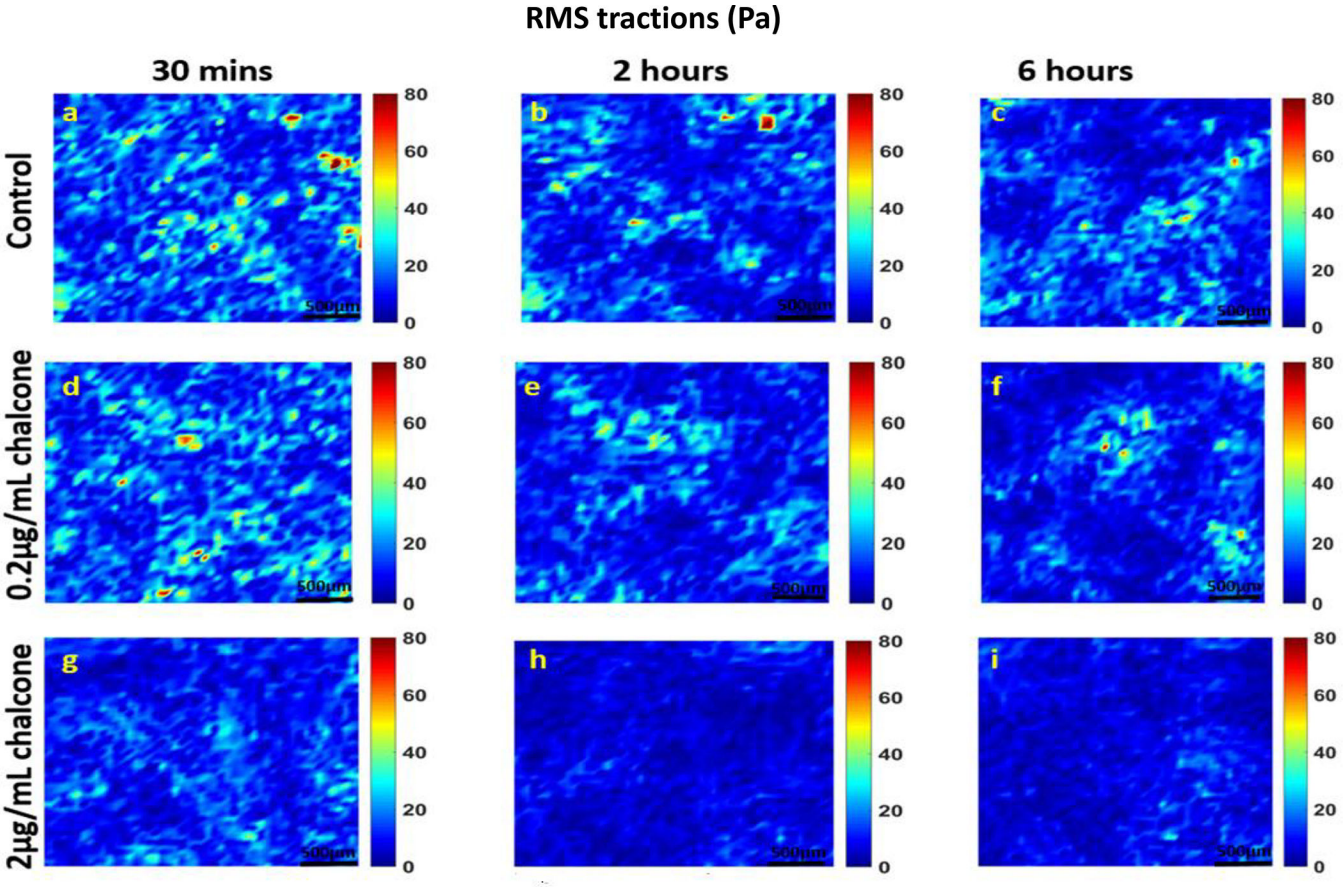

Figure 6:

rms traction (Pa) distributions of HUVEC monolayers during Cx43 disruption. Figure label shows control HUVECs (a, b and c), 0.2 µg/mL chalcone treated HUVECs (d, e and f) and 2 µg/mL chalcone treated HUVECS (g, h and i) at before any chalcone treatment (labels a, d and g), after 2 hours of experiment onset (labels b, e and h) and after 6 hours of experiment onset (labels c, f and i). Scale bar 500 × 500 µm.

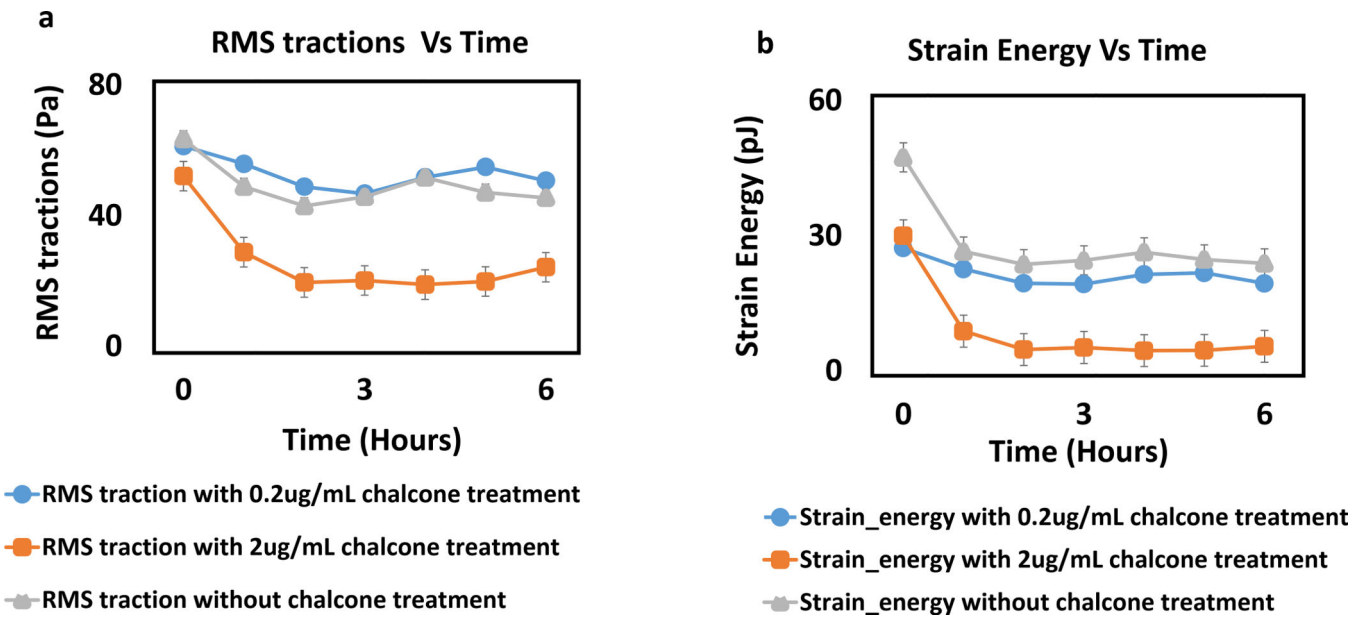

Figure 7:

rms tractions (Pa) (a) and strain energy (pJ) (b) in a HUVEC monolayer of both chalcone treated (0.2 μg/mL and 2 μg/mL) and control conditions. Error bars show standard error.

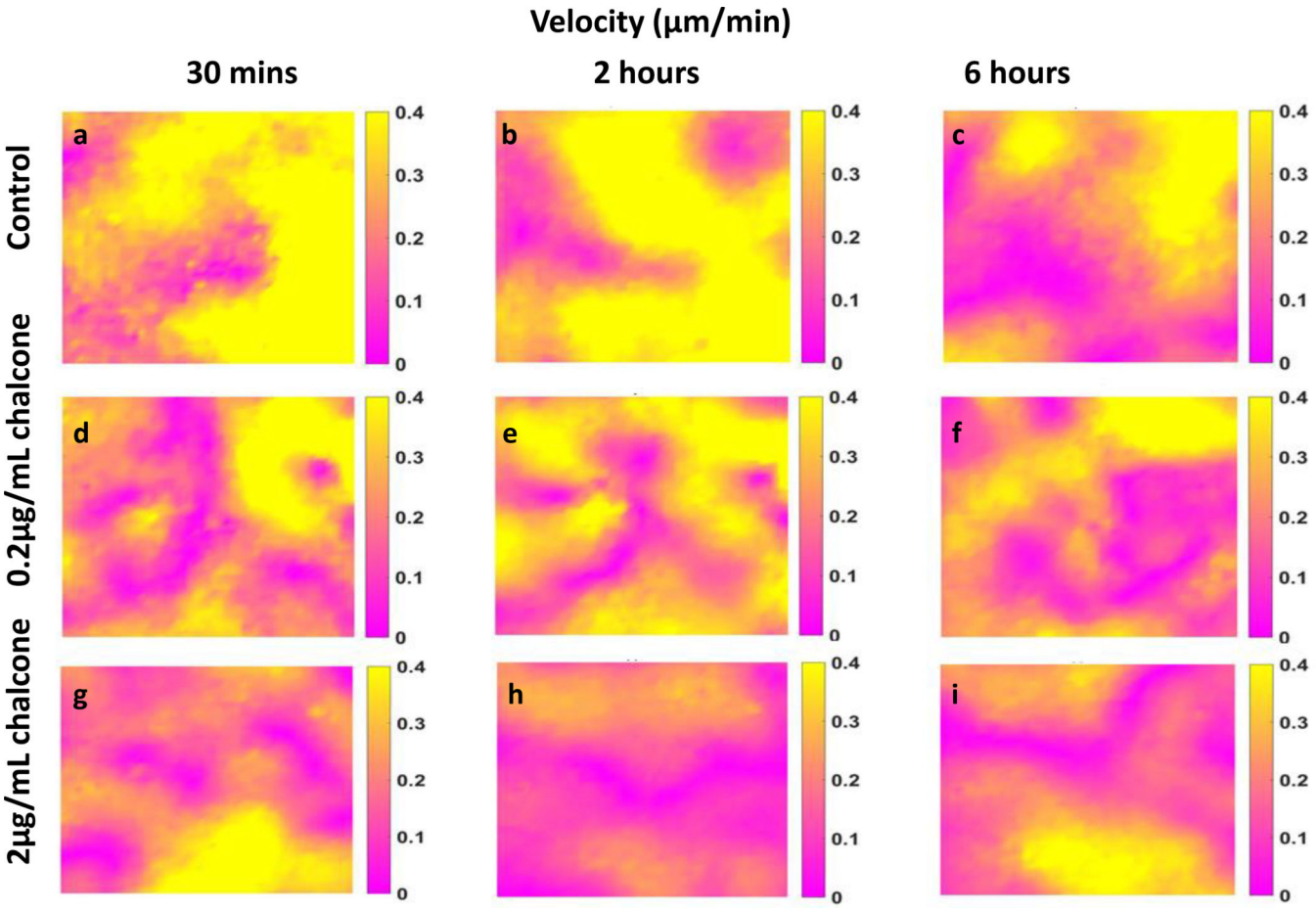

Figure 8:

Velocity in HUVEC monolayers during Cx43 inhibition. Figure labels are as follows—control (a, b and c), 0.2 μg/mL chalcone treated HUVECs (d, e and f) and 2μg/mL chalcone treated HUVECs (g, h and i) are showing velocity distributions at before chalcone treatment (labels a, d and g), after an hour of chalcone treatment (labels b, e and h) and at the end of experiment (labels c, f and i).

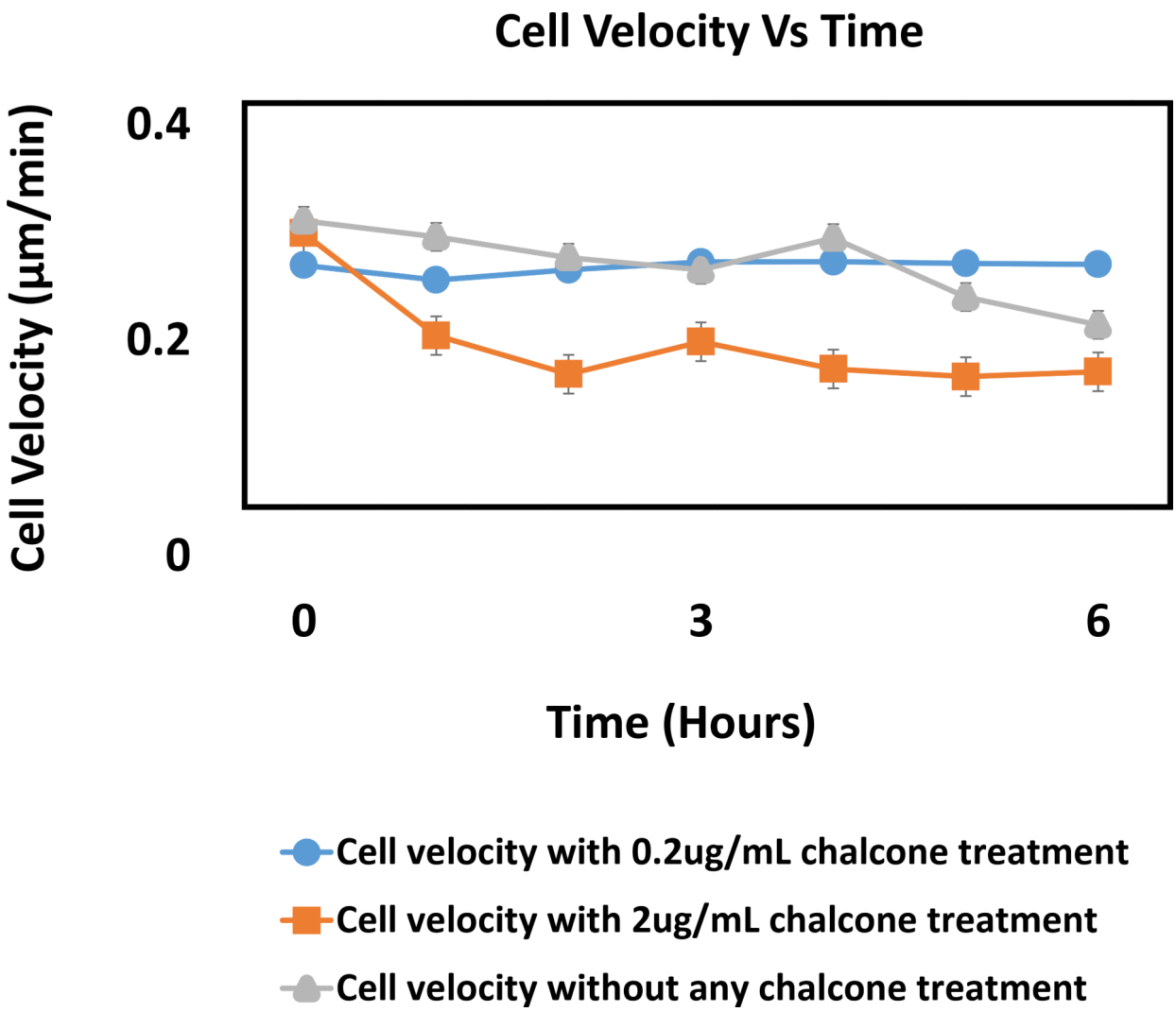

Figure 9:
Cellular velocity (µm/min) in a HUVEC monolayer of both chalcone treated (0.2 µg/mL and 2 µg/mL) and control conditions. Error bars show standard error.